· Article ·
doi: 10.13679/j.advps.2016.2.00107

Advances in Polar Science
June 2016 Vol. 27 No. 2: 107-116

PIV experimental study on the interactions between ice ridges and stratified fluids

TIE Wen, LU Peng*, LI Zhijun, LI Bo & WU Yan

State Key Laboratory of Coastal and Offshore Engineering, Dalian University of Technology, Dalian 116024, China

Received 6 March 2016; accepted 27 June 2016

Abstract With the rapid decline of Arctic sea ice, the freshwater produced by melting of summer sea ice makes the depth of the halocline under ice become shallower. This has an impact on the drift of sea ice because internal waves may be generated at the interface of the halocline by disturbance from the draft of an ice floe or ridge keel. A laboratory experimental study was carried out to investigate the interactions between an ice ridge and stratified fluid using the method of Particle Image Velocimetry (PIV). The drift velocity of an ice ridge (U) and the draft of the ridge keel (D) were altered in different experimental cases, and the velocity field in the stratified fluid was then measured by PIV. The results reveal that an obvious vortex exists in the wake field of the ridge keel, and the center of the vortex moves away from the ice ridge with increasing D. Internal waves at the interface of the stratified fluid were observed during the drift of the ice ridge, and the wave height shows a positive correlation with U and D. This study demonstrates that ice ridges could introduce internal waves at the interface of a stratified fluid and thus affect the oceanic drag coefficient and ice drift. It supports improved parameterization of the ice drag coefficients.

Keywords **Arctic sea ice, drag coefficient, stratified fluid, PIV, laboratory experiments**

Citation: Tie W, Lu P, Li Z J, et al. PIV experimental study on the interactions between ice ridges and stratified fluids. Adv Polar Sci, 2016, 27: 107-116, doi:10.13679/j.advps.2016.2.00107

1 Introduction

Sea ice is a key component of the global cryosphere, one of the most important indexes in the study of climate change, and the rapid decline of Arctic sea ice in recent years has drawn considerable attention[1]. Numerical simulation is the main method used to study Arctic sea ice. In this method, the ice dynamic model describes the exchanges in momentum between sea ice, the atmosphere, and the ocean, and the drag coefficients for the air-ice and ice-ocean interfaces are the key parameters in the ice dynamic model[2]. Parameterization of the sea ice drag coefficients in recent years has broken with the traditional methods that treated the drag coefficients as constant, and associated the coefficients with the spatial distribution conditions of sea ice[3]. Examination of the variable drag coefficients in ice dynamic models also showed better simulation results of sea ice drift if parameterized ice drag coefficients are employed[4]. However, the stratification of the ocean beneath the ice is not considered in the current parameterization of the ice-ocean drag coefficient[5-6]. In fact, the fresh water produced by the rapid melting of summer sea ice has driven the halocline shallower than before, especially in the marginal ice zone of the Arctic Ocean, where the halocline has been observed at a depth of 20 m or even shallower under ice[7]. In this situation, the drift of sea ice may introduce internal waves on the interface of stratified fluid, and so affect the oceanic drag force on the sea ice. In this way, the influence of the halocline on the drift of sea ice must not be ignored under the background of rapid ice melting in summer[8].

However, due to poor environmental conditions in the polar regions, it is very difficult to carry out in-situ observations on the flow field under ice. Physical modeling tests and other laboratory experiments can supplement these data and compensate for the limitations in weather conditions and measurement technology during the observations on the ice-ocean interface. The physical processes in sea ice dynamics can also be thoroughly investigated owing to man-made test conditions[9]. Particle image velocimetry (PIV) is the main non-contact method used to measure the velocity

* Corresponding author, E-mail: lupeng@dlut.edu.cn

field in fluids in the laboratory, it has been widely used in different studies because of its convenience and higher precision than other methods[10]. In this study, PIV was employed to investigate the interactions between ice ridges and stratified fluid and to evaluate the 2D velocity distribution under the ice. The experimental setup is first introduced, and then the velocity field and internal waves in different tests are discussed. Finally, the rules of variations in the velocity distribution in the stratified fluid are finally discussed to provide support for the impact of the shallow halocline on sea ice drift.

2 Experimental setup

The experiments were conducted in the PIV flume of the State Key Laboratory of Coastal and Offshore Engineering. The flow flume was 4.5 m long and 0.23 m wide, with a depth of 0.45 m, and a total water depth of 0.35 m. Pipelines with diameters of 2 cm were laid on the bottom of the flume, through small drain holes on the pipelines, and salt water can be injected into the flume after the fresh water on the upper layer is ready. The halocline under the ice was simulated in the flume using a two-layered fluid with a sharp interface separating the upper and lower layers. The salinity of the lower layer was 30 ppt, equaling the mean value of Arctic water. To visualize the two layers in the tests, the saline water was colored deep blue (Figure 1).

During the experiments, mixing on the interface between the two layers inevitably occurred due to internal

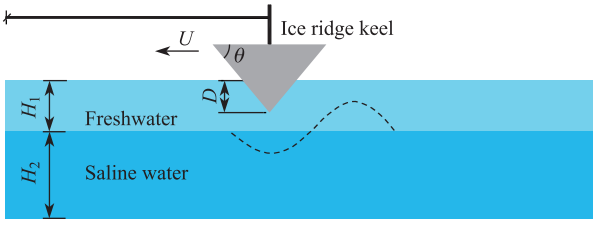

Figure 1 Schematic diagram of laboratory experiments on an ice ridge in a stratified fluid. The dashed lines on the interface between freshwater and saline water denote the internal waves due to the disturbance of the moving ridge keel in the stratified fluid. H_1 and H_2 are the depths of freshwater layer and saline water, respectively. D and θ are the respective draft and incline angle of the ice ridge keel. U is the moving speed of the ice ridge.

waves generated by the moving ridge keel. To maintain a clear interface before each test and to ensure the accuracy of the results, the following measures were taken: (1) an energy-dissipation network was placed at the ends of the flume to reduce the reflection of the internal waves; (2) a suitable time interval between adjacent tests was selected according to the drift velocity, in which the disturbed interface can be mostly recovered; (3) if the interface was largely disturbed and difficult to recover, then the stratified fluid in the flume was fully discharged and replaced by a new one. These measures preserved the sharpness of the halocline throughout the stratified tests.

Physical modeling tests of the ice ridge in the laboratory experiment were consistent with the dynamic similarity. As in most simulations, it is not possible to match all the relevant parameters. Here, because the primary interest is the effect of the internal wave on the stratified fluid, attention was placed on simulating the Froude number[11], defined as the ratio of inertial force to gravity. In terms of previous laboratory and field work, a length scale of 1:100 was employed in the Froude similarity between the full scale and the model scale in this study[12]. Field observations in the Arctic Ocean have revealed that the drift velocity of Arctic sea ice is usually within the range of 10—30 cm·s^{-1}[13], and the depth of the ice ridge keel is 2—10 m[14] with an incline angle of 10°—50°[15]. In addition, a shallow halocline has also been observed at MIZ in the Arctic at a depth of 15 m[7]. Based on these in-situ values and the selected length scale, in the experiments, the incline angle of the ridge keel model was $\theta = 45°$, and the draft of the ridge keel D was varied from 2 cm to 6 cm. The depth of the freshwater layer was $H_1 = 0.15$ m, and the saline water had a depth $H_2 = 0.2$ m. The speed at which the ice ridge moves, U, was varied from 1 cm·s^{-1} to 30 cm·s^{-1}. Here, some higher velocity values ($U > 3$ cm·s^{-1}) were employed to improve the integrity of the experimental data and facilitate understanding of the physical mechanisms under different flow patterns from subcritical through fully supercritical[11].

The ridge keel model was made of plexiglass, with a cross-section of inverted isosceles triangles. Small tracks and a movable platform used to fix the ridge keel model were installed in the flow flume, and the platform was linked to an electric motor by a wire rope, so that the velocity of the platform could be changed by turning the rotation rate of the motor. The draft of the ridge keel model into the freshwater layer could be also altered by changing the installation height of the model on the platform, as shown in Figure 2.

The basic steps of the PIV method are as follows: (1) The fluid was seeded with tracer particles which are assumed to faithfully follow the flow dynamics. (2) A laser beam was expanded into a plane, entering the fluid, so that the particles with a thin sheet of the fluid were illuminated and visible. (3) A camera with the lens perpendicular to the laser plane captured the illuminated particles at high frequency f, and two frames with very short time interval (Δt) were obtained at each time. (4) A process called cross-correlation was employed to analyze the two frames, and the displacement of the particles in Δt could be determined, which in turn allowed determination of their velocity. The PIV experimental equipment is shown in Figure 2. Considering the symmetry of flow in the flume and the lack of any obvious variation in velocity along the direction of ridge width, only the two-dimensional velocity field was measured in the experiment. For different drift velocities of the ridge model, different values for f and Δt were selected to produce clear results with respect to flow visualization, and the total number of frames N was determined by the time period in which the ridge model was within the visual field of the camera. All values are summarized in Table 1.

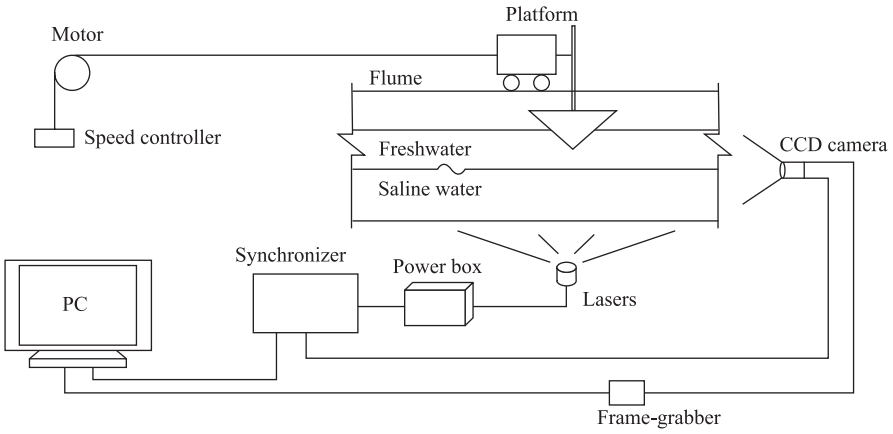

Figure 2 Equipment used for the PIV experiment.

Table 1 Drift velocity of ridge model, Δt and the total frames N

U/ (cm·s^{-1})	3	6	7	8	9	10	12	15	18	24	30
Δt /μs	9000	8000	5000	2500	2000	1800	1600	1500	1200	1000	900
N	400	250	250	200	200	150	150	150	100	100	80

The selection of the tracer particles is very important for the precision of the measurements of the PIV experiment. Except for the requirements of innocuity, noncorrosivity, and chemical stability, the tracer particles should satisfy the requirements of light scattering and flow following features. The sedimentation velocity, w, is an important index to describe the following features of the tracer particles:

$$w = \frac{d_s^2 g(\rho_s - \rho)}{18\mu} \quad (1)$$

Here, d_s and ρ_s are the respective diameter and density of the tracer particles, and ρ and μ are the respective density and kinematical viscosity of the fluid[17].

In this study, polystyrene powder with a diameter of 50 μm and a density of 1.055×10^3 kg·m^{-3} was selected for the tracer particles, and the sedimentation velocity was determined as $w = 7.47\times10^{-3}$ cm·s^{-1} in freshwater and $w = 2.72\times10^{-3}$ cm·s^{-1} in saline water. Both values are lower than the drift velocity of the ridge model by more than 3 orders of magnitude, satisfying the precision requirements.

3 Experimental results

3.1 Velocity field in a stratified fluid

Observations on the flow field focused mainly on the wake field behind the ridge keel and the interface within the stratified fluid. The draft of the ridge keel model D was set to 2, 4, and 6 cm, the draft to the upper layer depth ratio, D/H_1 ranged from 0.13 to 0.4 in different tests, and the velocity of the ridge model U was set to 3, 6, 7, 8, 9, 10, 12, 15, 18, 24, and 30 cm·s^{-1} for each draft value, totaling 33 cases. The non-dimensional Reynolds number is defined as: $R_e = UD/v$, where v is the fluid's kinematic viscosity. The PIV imagery was pre-processed using INSIGHT 4G and then post-processed using TECPLOT, as shown in Figure 3.

As shown in Figure 3b, a vortex exists near the lee side of the ridge keel; the disturbance of the ridge keel in the flow field was only within the range close to the ridge keel, and the flow velocity reduces gradually beyond that range. The shielding effect of the ridge keel on the following flow field is the main reason for this phenomenon, and the wake field due

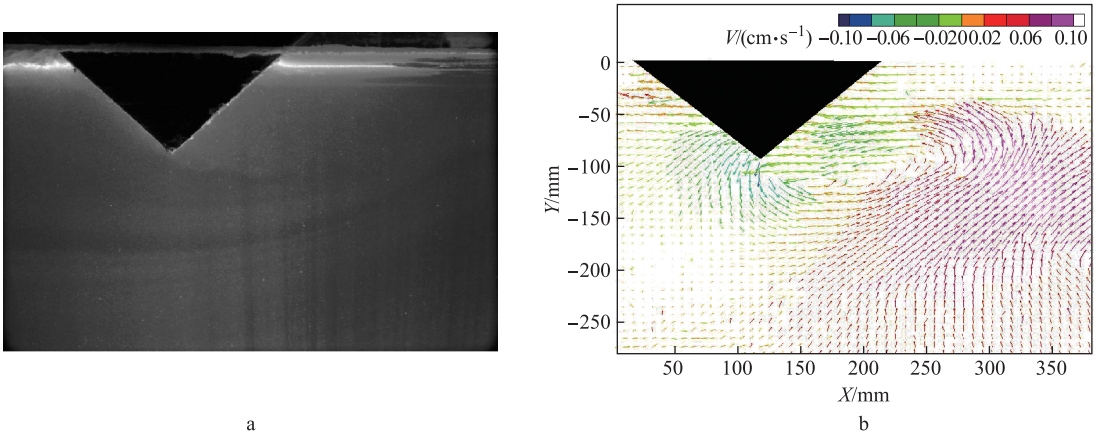

a b

Figure 3 PIV imagery of the ridge keel for D=6 cm and U=6 cm·s^{-1} (R_e = 3214). **a**, Ridge keel model; **b**, PIV imagery of the ridge model.

to the shielding effect can directly affect the drag force on the ridge keel. This is an important aspect of the parameterization of the sea ice drag coefficients.

Figure 4 shows the streamline plot of the flow field at the same velocity (U = 15 cm·s^{-1}) for three different ridge keel drafts (D = 2, 4, 6 cm). The results show that under the same velocity, the range of the vortex in the wake field increased markedly with the increasing draft of the ridge keel, and the center of the vortex also gradually drifted away from the lee side of the ridge keel. This is mainly attributed to the enhanced shielding effect on the wake field as the greater part of the ridge keel became immersed in the fluid.

The streamline plot of the flow field with the same draft (D = 6 cm) and six different velocities (U = 3, 8, 12, 15, 24, 30 cm·s^{-1}) is shown in Figure 5. The difference between Figure 4 and Figure 5 is obvious. The range in vortex also increased with increasing velocity, but the difference was not as pronounced, and multiple vortex centers occurred in the wake field as the drift velocity increased to a certain level, such as the Karman vortex street behind a cylinder. According to a previous study[18], when h/L=0.281 (where h is the width between the two vortex columns, and L is the distance between the two vortices) and R_e=150, the Karman vortex street was stable. The shedding frequencies of the Karman vortex street behind a cylinder were proportional to the velocity when the R_e was within a range from 200 to 15000.

To evaluate the influence of the drift of the ridge keel

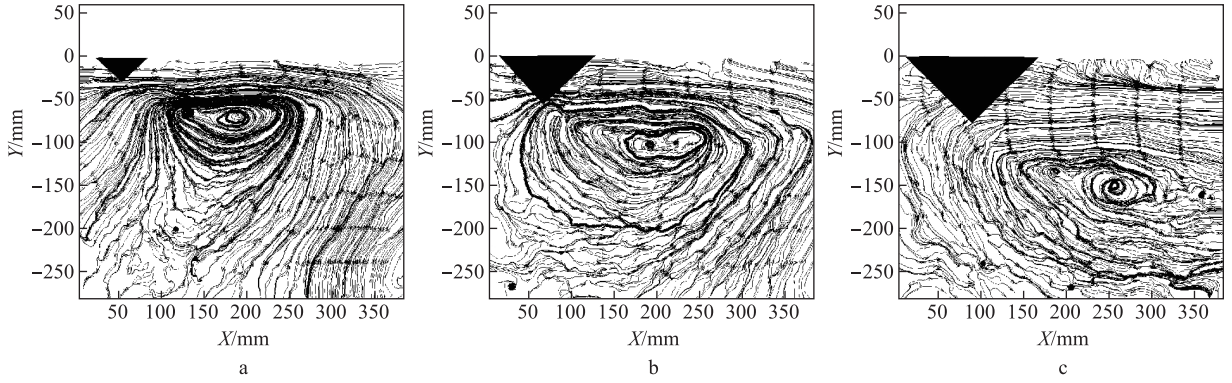

Figure 4 Streamline plot of the flow field under the same velocity (U=15 cm·s^{-1}). **a**, D=2 cm (R_e = 2679) ; **b**, D=4 cm (R_e = 5357); **c**, D= 6 cm (R_e = 8036).

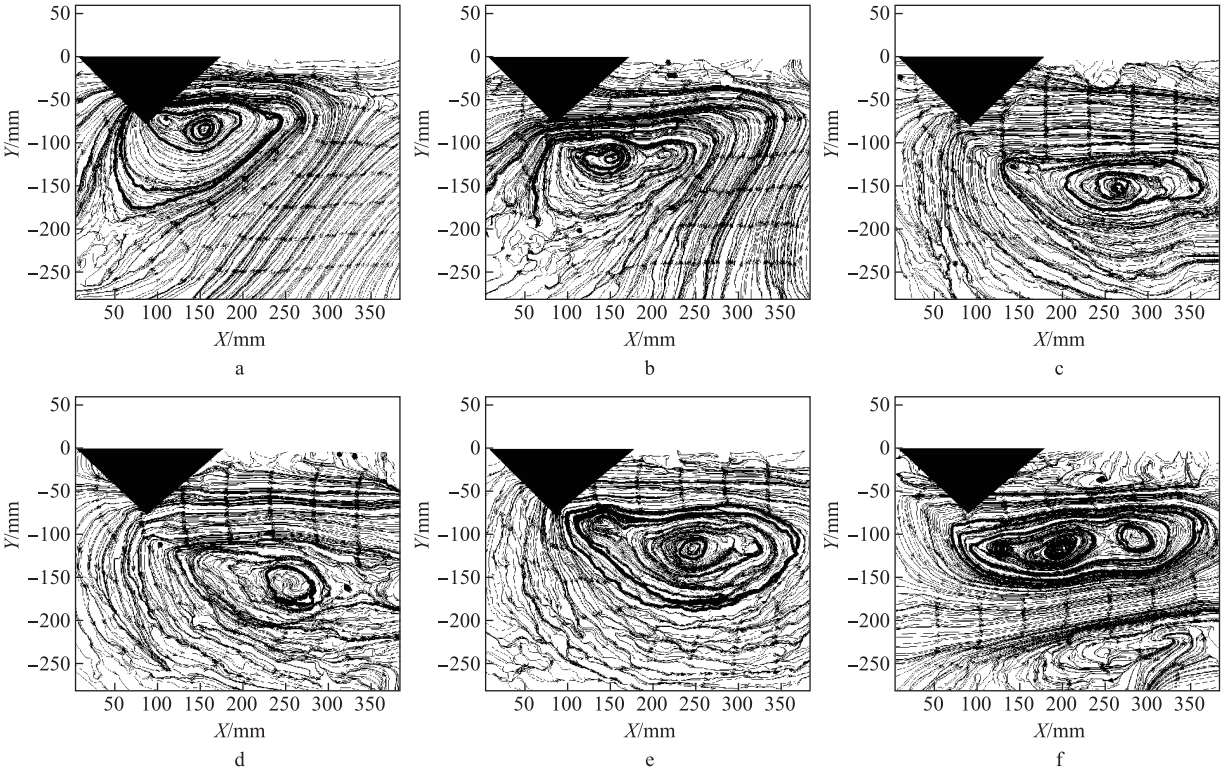

Figure 5 Streamline plot of the flow field under the same draft (D=6 cm). **a**, U=3 cm·s^{-1} (R_e =1607); **b**, U=8 cm·s^{-1} (R_e =4286); **c**, U= 12 cm·s^{-1} (R_e =6429) ; **d**, U=15 cm·s^{-1} (R_e =8036); **e**, U=24 cm·s^{-1} (R_e =12857); **f**, U=30 cm·s^{-1} (R_e =16071).

on the vortex, the distance from the center of the vortex to the sharp corner of the ice ridge keel T was determined. If multiple vortexes were present in the wake field of the ice ridge, the average distance from these vortex centers to the sharp corner of the ice ridge was used. Variations in the horizontal and vertical distances (T) with the two impact factors, U and D, for different experimental cases are shown in Figure 6.

As noticed in Figure 6a, with the increasing draft of the ice ridge, the center of the vortex drifted away from the ridge keel not only in the horizontal direction but also in the vertical direction, sinking deeper into the fluid. In this way, it became easier to disturb the interface in the stratified fluid than in cases with shallower draft.

Figure 6b shows the horizontal and vertical distances (T) from the center of the vortex to the sharp corner of the ice ridge with the increasing velocity, and the expansion of the vortex range took place mainly in the horizontal direction rather than in the vertical direction. That is, a series of vortexes were observed at higher velocity (Figures 5e, 5f), similar to that of the Karman vortex street behind a cylinder[18], and the horizontal scale of the wake field was greatly extended. However, the increase in the horizontal distance was only obvious for low velocity, and then remained nearly constant as U >-15 cm·s^{-1}. This was partially because the range of the vortex streets for large Reynolds numbers (R_e > 8036) extended the scope of the PIV measurements in the experiments. The change in the relative depth of the vortex was much less pronounced than the changes in horizontal distance, except for a slight increase for small Reynolds numbers (Figure 6b), indicating a nearly constant influence of drifting velocity on the depth of the vortex center in the stratified fluid.

3.2 Internal waves

In the experiments concerning ridge keels in the stratified fluid, internal waves on the interface between the two layers with different density were clearly observed as the ridge drifted. For this reason, the Froude number should be defined

$$F_r = \frac{U}{U_0} \tag{2}$$

in the stratified fluid for discussions on the internal waves:

Here, U is the model velocity, and U_0 is the internal wave phase velocity. For a horizontally propagating, shallow water gravity wave in a two-layer, inviscid fluid, the relationship for U_0 can be written as follows:

$$U_0^2 = \frac{g(\rho_2 - \rho_1)}{\rho_2} \frac{H_1 H_2}{H_1 + H_2} \tag{3}$$

Here, ρ_2 is the density of saline water, and other variables are defined as above. U_0=0.13 m·s^{-1} was determined here using the corresponding previously defined value[19].

To determine the flow velocity field and internal waves, each test case was performed twice, once for the PIV measurement and then for video recording, which allows comparison of the PIV flow field and the internal waves captured by video. If the position and time of the PIV imagery are known, the internal wave surface can be determined from the corresponding video snapshot, as shown in Figure 7. The dashed lines were first identified on an enlarged portion of the snapshots of internal waves taken from video screenshots, and then copied to the corresponding position of PIV imagery. Figure 7 shows the internal waves in the stratified fluid captured by the video snapshots as the velocity of the ice ridge U=3 cm·s^{-1} and draft D=2, 4, and 6 cm, corresponding to a ratio of draft to upper layer depth, D/H_1, which ranged from 0.13 to 0.4. The results show that the internal wave height (K) increased with increasing D/H_1, and the wave peak also gradually approached the lee-side of the ridge keel.

Figure 8 shows the snapshots of internal waves and corresponding flow fields for constant D/H_1=0.4 and U = 3, 6, 9, 15, 24, and 30 cm·s^{-1}, with corresponding Froude number ranging from 0.23 to 2.31. The results show that, as the velocity of the ice ridge increased, the range of influence of the internal waves on the flow field also increased considerably because of the increasing internal wave height (K), but the wave peak gradually drifted far from the lee-side of the ridge keel. The flow velocity visibly enhanced the wake field of the ice ridge at Froude numbers ranging from 0.5 to 0.7, and there was high vortex intensity. When the Froude number was either below 0.5 or greater than 0.7, the

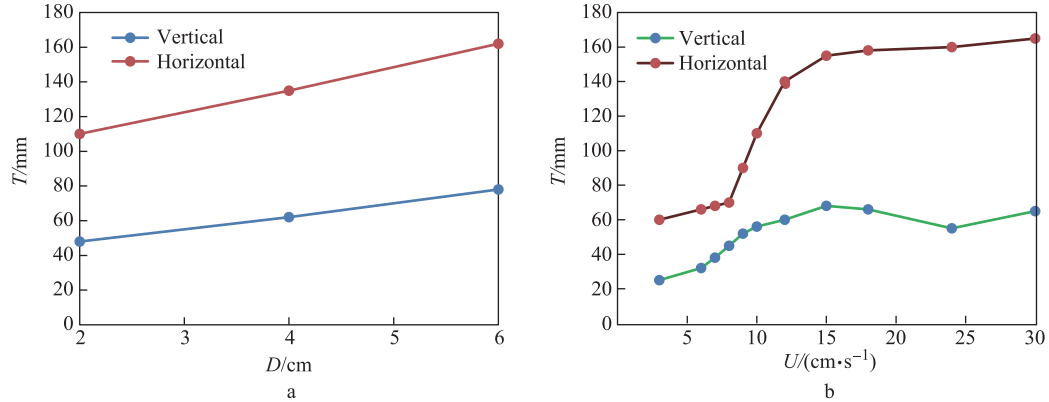

Figure 6 The horizontal and vertical distances (T) from the vortex center to the sharp corner of the ice ridge. **a**, At the same velocity (U= 15 cm·s^{-1}); **b**, At the same draft (D=6 cm).

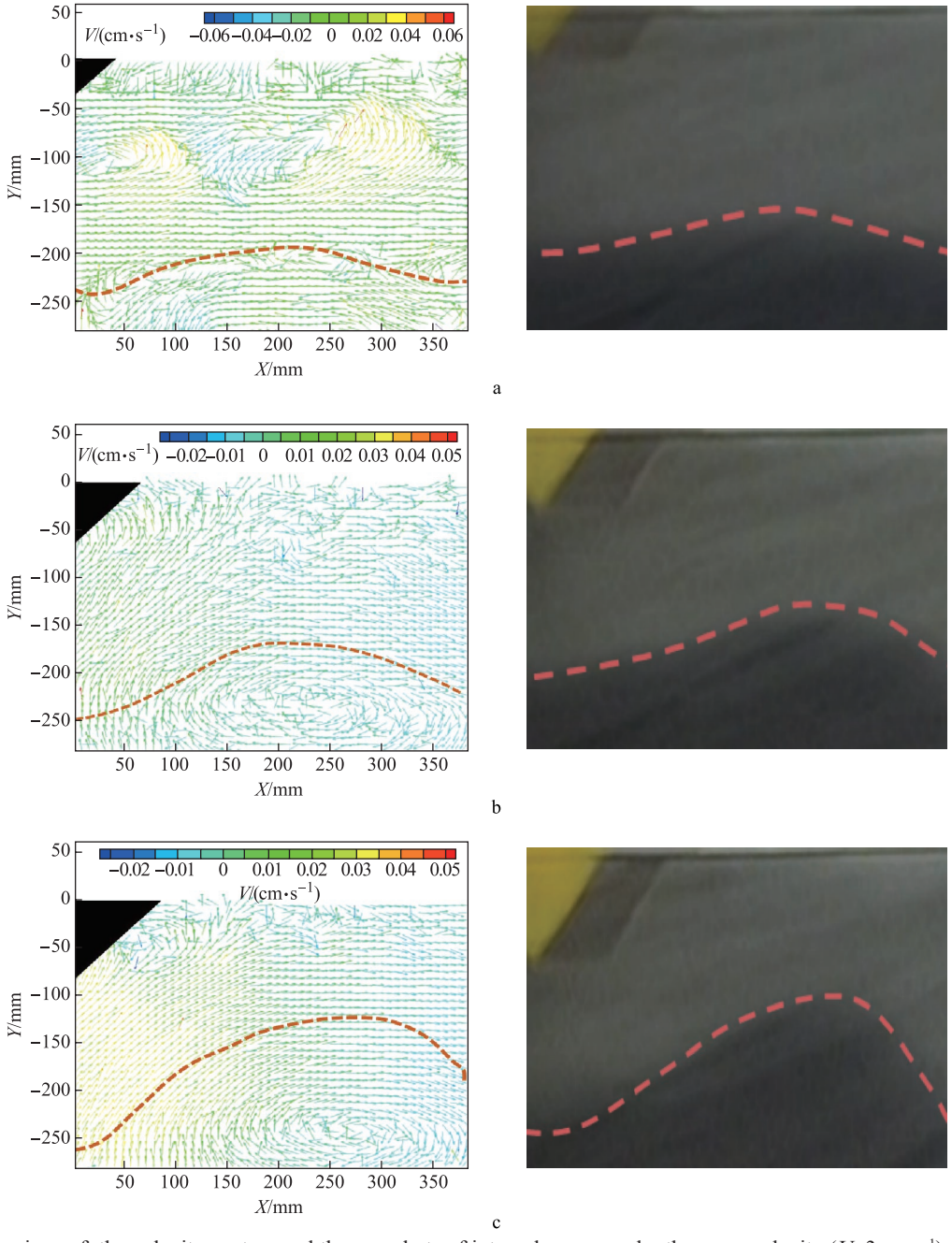

Figure 7 Comparison of the velocity vectors and the snapshots of internal waves under the same velocity (U=3 cm·s^{-1}). **a**, D/H_1=0.13; **b**, D/H_1=0.26 ; **c**, D/H_1=0.4.

vortex intensity in the wake field was relatively weak. This phenomenon may be due to the production of the turbulent mixing evident in the wake of the ice ridge, which clearly adds significant resistance[19].

To quantitatively study the influence of impact factors on the internal waves, the correlation between wave height (K) and the ratio of D/H_1 and the Froude number was obtained. Figure 9 shows the variation of wave height (K) with non-dimensional parameters. Here, wave height K refers to the vertical distance between the adjacent peaks and troughs, and the vertical distance is the nearest to the ridge keel. It is clear that with increased D/H_1, the wave height increased monotonically and the shielding effect of the ridge keel on the following fluid increased at the same velocity (Figure 9a). A similar phenomenon was observed in the region of attenuation of the flow velocity behind the lee-side of the ridge keel, shown in Figure 4.

The results also showed that the internal wave height increased with the increasing Froude number for a constant ratio of D/H_1 (Figure 9b), but the change in wave height was not monotonic. A rapid increase in wave height with velocity began at F_r≈0.2; a local maximum in wave height occurred at F_r≈0.7 and then decreased for Froude numbers ranging from 0.7 to 1.2. After a minimum, the wave height increased

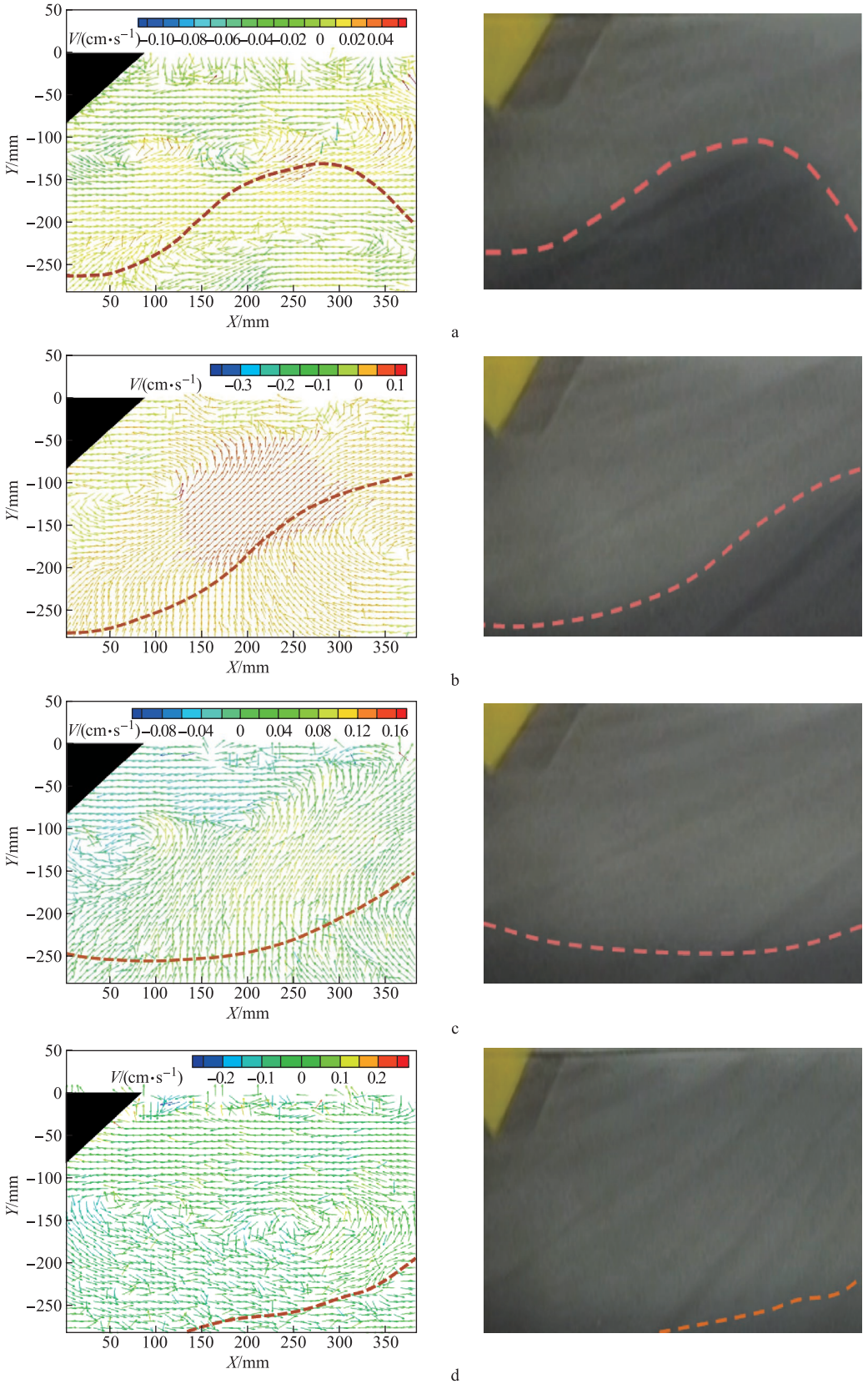

Figure 8 Comparison of the velocity vectors and snapshots of internal waves at the same D/H_1=0.4. **a**, Velocity of the ice ridge U= 3 cm·s^{-1} and F_r=0.23; **b**, Velocity of the ice ridge U=6 cm·s^{-1} and F_r=0.5; **c**, Velocity of the ice ridge U=9 cm·s^{-1} and F_r=0.7; **d**, Velocity of the ice ridge U=15 cm·s^{-1} and F_r=1.2.

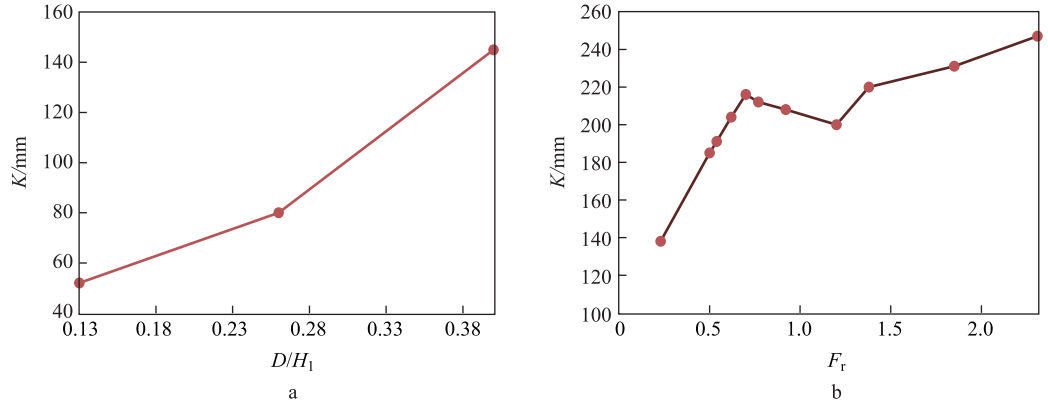

Figure 9 Variations in wave height (K) with non-dimensional parameters D/H_1 and F_r. **a**, At the same velocity U=3 cm·s^{-1} and F_r=0.23; **b**, At the same draft D=6 cm and D/H_1=0.4.

monotonically as the Froude number increased, but the increase in speed was less pronounced than at the beginning of the scenario. The non-monotonic variations in internal wave height may impact the drag force on the ridge keel, as discussed below.

4 Discussion

The internal waves observed in the PIV measurements of course impacted the drag force on the ridge keel model. Measurements on the drag force were also made in the concurrent experiments, but they were not the focus of this study. However, there are still some matters to discuss regarding the relationship between the internal waves, the drag force, and the drag coefficient.

A detailed discussion on the drag force on the ridge keel in uniform fluid and stratified fluid was presented in a previous work[20], and Figure 10 provides the measurements of the drag force corresponding to the cases in this study. These were also included in the comparisons with the results obtained for a uniform fluid.

As shown in Figure 11, the drag force on the ridge keel in a stratified fluid was significantly different from that in a uniform fluid. The drag forces in the uniform fluid and stratified fluid were small if the velocities of the ice ridge were low. As the speed increased, the drag force in the stratified fluid increased more rapidly, peaking at about 6 cm·s^{-1} to 9 cm·s^{-1}, after which the drag force gradually decreased, reaching a minimum at about 9 cm·s^{-1} to 11 cm·s^{-1}. In this process, the stratified drag force was greater than the uniform drag force. As the velocity continued to increase (>11 cm·s^{-1}), the stratified drag force and uniform drag force gradually converged.

$$C_t = \frac{F}{A\rho U^2} \tag{4}$$

The sea ice drag coefficient C_t was found to be easily determined using the drag force:

Here, F is the ice ridge drag force, A is the projected area of the model over the fresh water along the direction of motion, and ρ is the density of the fluid[20]. The results of the drag coefficient for the stratified fluid and uniform fluid are plotted versus Froude number in Figure 11.

The results showed that the drag coefficient in the stratified fluid increased gradually with the Froude number before a peak of C_t at $F_r \approx 0.4$. When the Froude number exceeded 0.6, the drag coefficient in the stratified fluid decreased visibly with F_r and then approached a similar value with the corresponding value in the uniform fluid, and was

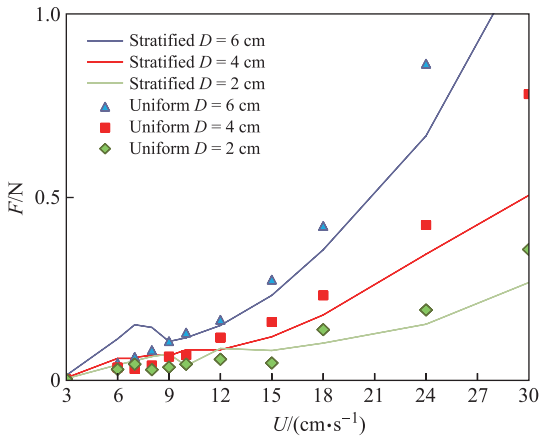

Figure 10 Drag force on the ridge keel in the stratified fluid, and comparison with results for a uniform fluid.

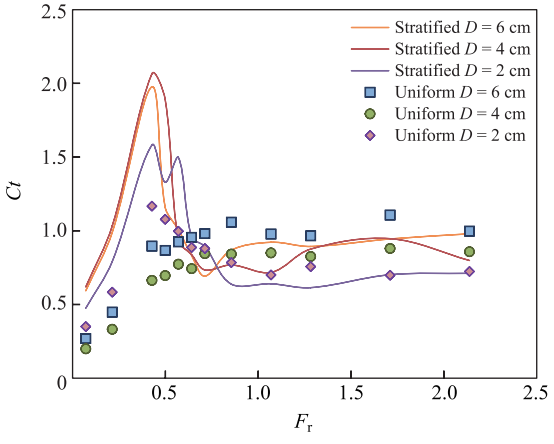

Figure 11 Drag coefficient of the ridge keel in the stratified fluid, and comparisons with the results in the uniform fluid.

nearly constant with respect to F_r.

The velocity vector diagram (Figure 8) provides some explanations regarding the non-monotonic variations in the measured drag coefficient. As velocity increased, the area of influence of the internal waves increased gradually. When the velocity of the ice ridge was 6 cm·s^{-1} (F_r=0.4) to 9 cm·s^{-1} (F_r=0.6), the flow velocity became more pronounced in the wake field of the ice ridge than elsewhere. Within the velocity range of 6 cm·s^{-1} to 9 cm·s^{-1}, the stratified fluid drag force and drag coefficient changed non-monotonically and increased more significantly than the uniform fluid's coefficient. This was mainly due to internal waves in the stratified fluid sparked by movement of the ridge. It is still surprising that the peak drag coefficient occurred at $F_r \approx$ 0.4—0.6 because intuitively, the maximum energy transfer would be expected to occur when the velocity of the ice ridge was equal to the internal wave phase speed, namely F_r=1. However, this was also observed in previous studies[19], possibly because the internal wave on the interface is actually a combination of different wave modes rather than solely the internal wave with a first-mode phase speed as defined in equation (3).

5 Conclusion

In this paper, the interaction between an ice ridge keel and stratified fluid was studied using laboratory experiments, and PIV technology was used to measure the velocity field in the flow under ice. The velocity field in the flow under ice and its variations with different factors were studied by changing the draft and moving speed of the ridge keel model. The main conclusions are as follows:

(1) The influence of the ridge keel on the stratified fluid was found to be limited within a small region near the lee-side of the ridge keel. Vortexes were observed in the wake field behind the lee-side of the ridge keel model, and the flow velocity attenuated in the wake field. However, beyond the range of the wake field, the disturbance on the fluid was negligible. For a constant drift velocity (U > 20 cm·s^{-1}), the range of the vortex increased with the increasing draft of the ridge keel, and the center of the vortex gradually drifted far from the lee-side of the ridge keel. For a constant draft, multiple vortex centers were observed in the wake field as the drift velocity increased to a certain level, but the changes in the vortex range were not clearly different for different drafts.

(2) Movement of the ice ridge on the water surface can cause internal waves on the interface between two layers of different densities within the stratified fluid. For a constant drift velocity of the ice ridge, the internal wave height increased with the draft to an upper layer depth ratio of the ridge keel (D/H_1). For a constant D/H_1, the internal wave height also increased with the drift velocity. The internal wave placed external resistance on the ridge keel, and variations in the drag force on the ridge keel in the stratified fluid were rendered non-monotonic for different Froude numbers, further proving the impact of the stratified fluid on the drag coefficient of the ice ridge.

Because of the limitations of the experimental conditions, only a ridge model (α = 45°) in a constant stratified fluid (H_1 = 0.15 m, H_2 = 0.2 m) was considered. More situations should be considered in further studies. For example, different tile angles of the ridge keel model, and different combinations of the depth and density of the stratified fluid should be introduced, which may provide a clearer description of the influence of a shallower halocline on the drift of Arctic sea ice, and then provide evidence for the development of parameterization of the sea ice drag coefficients.

Acknowledgments This study was supported by the National Natural Science Foundation of China (Grant nos. 41276191, 41306207, 41376186).

References

1 Shen Y P, Liang H. Global ice melting accelerated would threaten to human environmental safety. J Glaciol Geocryol, 2011, 23(2): 208–211 (in Chinese)
2 Ji S Y, Yue Q J. Numerical simulation of sea ice in engineering and its applications. Beijing: Science Press, 2011 (in Chinese)
3 Zhang Q. Application of PIV on flow field measurement under floe ice in laboratory modeling. Dalian: Dalian University of Technology, 2009 (in Chinese)
4 Tsamados M, Feltham D L, Schroeder D, et al. Impact of variable atmospheric and oceanic form drag on simulations of Arctic sea ice. J Phys Oceanogr, 2014, 44(5): 1329–1353
5 Lüpkes C, Gryanik V M, Rösel A, et al. Effect of sea ice morphology during Arctic summer on atmospheric drag coefficients used in climate models. Geophys Res Lett, 2013, 40(2):466–451
6 Lu P, Li Z J, Cheng B, et al. A parameterization of the ice-ocean drag coefficient. J Geophys Res, 2011, 116(C7): C07019
7 Shi J X, Zhao J P. Advances in studies on the Arctic halocline. Adv Earth Sci, 2003, 18(3): 351–357 (in Chinese)
8 Zhang L, Zhang Z H, Li Q, et al. Status of the recent declining of Arctic sea ice studies. Chin J Polar Sci, 2010, 21(1): 71–80
9 Lu P. Study on sea ice geometric parameters and parameterization of drag coefficient based on image analysis. Dalian: Dalian University of Technology, 2007 (in Chinese)
10 Adrian R J. Particle-imaging techniques for experimental fluid mechanics. Annu Rev Fluid Mech, 1991, 23(1): 261–304
11 Prre H D, Topham D R, Van Hardeenberg B J. Laboratory measurements of the drag force on a family of two-dimensional ice keel models in a two-layer flow. J Phys Oceanogr, 1995, 25(12): 3008–3031
12 Topham D R, Pite H D, Johnston P J, et al. Stratified flows generated by an arctic ice keel. Preprints, Third Int. Symp. On Stratified Flows. Pasadena, CA: ASCE, 1987: 975–984
13 Alexandrov V Y, Martin T, Kolatschek J, et al. Sea ice circulation in the Laptev Sea and ice export to the Arctic Ocean: results from satellite remote sensing and numerical modeling. J Geophys Res, 2000, 105(C7): 17143–17159
14 Martinson D G, Wamser C. Ice drift and momentum exchange in winter Antarctic pack ice. J Geophys Res, 1990, 95(C2): 1741–1755
15 Li J, Bai Y L, Li X J, et al. Statistics and studies on morphological characteristics of two kinds of typical ice ridge in Antarctic Weddell Sea. J Bohai Univ (Nat Sci Ed), 2011, 32(2): 100–104 (in Chinese)
16 Bourke R H, McLaren A S. Contour mapping of Arctic Basin ice draft and roughness parameters. J Geophys Res, 1992, 97(C11): 17715–

17728
17 Yuan C, Sun C D, Bai Y L, et al. The characteristics of the tracer particles used in water flow field for PIV system. J Exp Fluid Mech, 2006, 20(2): 72–77 (in Chinese)
18 Hou H C. Preliminary analysis and application on Karman swirl. J Qinghai Normal Univ (Nat Sci), 2005, (3): 23–25 (in Chinese)
19 Waters J K, Bruno M S. Internal wave generation by ice floes moving in stratified water: results from a laboratory study. J Geophys Res, 1995, 100(C7): 13635–13639
20 Li B, Wu Y, Lu P. An experimental study on ice ridge drag coefficient in stratified fluid. Proceedings of the 17th China ocean engineering academic discussion. Nanning, 2015: 317–321 (in Chinese)